Design and Implementation of a Tunable 40 MHz-70 MHz Gm-C Bandpass $\Delta\Sigma$ Modulator

Omid Shoaei, *Member, IEEE,* and W. Martin Snelgrove, *Member, IEEE*

Abstract-The discrete-time $\Delta\Sigma$ modulator is transformed to the continuous-time $\Delta\Sigma$ modulator. For either nonreturn to-zero or return to-zero feedback, the loop transfer functions of the continuous-time and discrete-time modulators can be made exactly equivalent. Hence, a stable discrete-time $\Delta\Sigma$ modulator is mapped to a stable continuous-time $\Delta\Sigma$ modulator having the same SNR. The anti-alias (image rejection) properties of the continuous-time modulator are described. Experimental results for a tunable 40 MHz-70 MHz continuous-time Gm-C modulator are shown to verify the theory. A master-slave tuning scheme is developed to tune the Gm-C $\Delta\Sigma$ loop filter.

Index **Terms-Analog-to-digital converter, bandpass $\Delta\Sigma$ ADC's, continuous-time filtering, converter, $\Delta\Sigma$ modulator.**

I. INTRODUCTION

A SWITCHED-C technique for bandpass $\Delta\Sigma$ modulators was introduced in [1] and later implemented for two different IF frequencies, 455 KHz [2] and 10.7 MHz [3]. The demand for high-speed $\Delta\Sigma$ oversampling analog-to-digital conversion especially for bandpass signals makes it necessary to look for a technique that is faster than switched-C. This demand has stimulated researchers to develop a method for designing continuous-time $\Delta\Sigma$ A/DS, which can be much faster than their switched-C counterparts. Early designs of continuous-time bandpass modulators were approximate, guided by the intuition that replacing "integrators" with "resonators" should make a bandpass converter [4]-[6]. However, because of the lack of an exact design theory designers had to spoil the Q of their resonators to make the loop stable, which reduced the effectiveness of noise shaping. In [6], for example, adding a damping factor causes the fourth-order $\Delta\Sigma$ to behave more or less as a second-order system.

An exact design for a continuous-time modulator was reported recently [7]-[9]. It was shown that a continuous-time $\Delta\Sigma$ loop can be designed entirely in the discrete-time domain and the same noise shaping behavior obtained for either continuous-time or discrete-time $\Delta\Sigma$ loops. Therefore, one can determine the performance of the $\Delta\Sigma$ loop, including stability and SNR, from the original discrete-time modulator. Then by applying the transformation presented in [7] and [8] an exactly equivalent continuous-time modulator will be obtained.
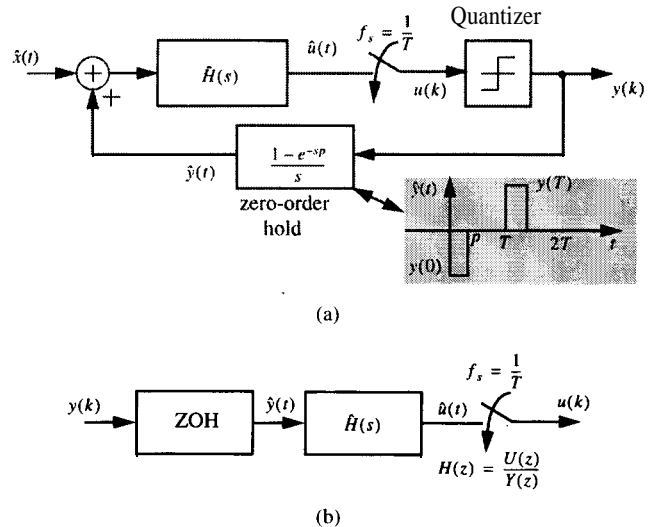
Fig. 1. (a) Continuous-time $\Delta\Sigma$ modulator. (b) $\Delta\Sigma$ open loop block diagram.

In this paper it is theoretically and experimentally shown that a continuous-time modulator provides anti-alias filtering for out-of-band signals. Moreover, a master-slave tuning scheme has been used to tune an integrated continuous-time Gm-C filter inside the $\Delta\Sigma$ modulator loop.

An overview of this paper is as follows. A more detailed presentation of the transformation from a discrete-time to a continuous-time modulator shown in [7] is given in Section II. The implicit anti-alias filter associated with a continuous-time modulator, which gives an inherent system advantage relative to a switched-C technology, is discussed in Section III. The continuous-time second-order Gm-C bandpass $\Delta\Sigma$ modulator prototype and experimental results including the tuning scheme are given in Sections IV and V, respectively. The prototype consists of two integrated 0.8 μm BiCMOS Gm-C filters, one in the modulator loop (slave), the other working as a (master) VCO and off-chip tuning circuitry. This modulator has been tuned from 40 to 70 MHz with clocks at four times the band center.

II. TRANSFORMATION OF DISCRETE-TIME $\Delta\Sigma M$ TO CONTINUOUS-TIME $\Delta\Sigma M$

A block diagram of a continuous-time $\Delta\Sigma$ modulator is shown in Fig. l(a) [7]. The filter loop is represented by H(s) and the DAC transfer function by a zero-order-hold (ZOH) in which p is the opening aperture. For a return-to-
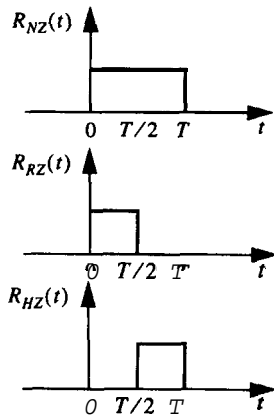
Fig. 2.   NRZ, RZ, and HZ DAC feedback impulse responses.

zero (RZ) DAC $p = T/2$, and for a nonretum-to-zero (NRZ) DAC $p = T$, where T is one sampling period. A RZ DAC reduces the nonlinearity due to the fact that the area under a practical pulse depends on the levels of the preceding and following pulses [10]. Fig. l(b) shows the $\Delta\Sigma$ signal path from the output of quantizer back to its input. As can be seen from Fig. l(b) the overall $\Delta\Sigma$ loop gain is a discrete-time function, so one can derive the exact discrete-time transfer function, $\mathrm{II}(z)$, of the loop given the transfer functions of the continuous-time loop filter, $\hat{H}(s)$, and the ZOH as follows:

$$\mathcal{Z}^{-1}[H(z)] = \mathcal{L}^{-1}\left[\frac{1 - e^{-sp}}{s}\hat{H}(s)\right]\Bigg|_{t=nT} \tag{1}$$

Equation (1) can be expressed in the time domain by

$$h(nT) = [p_T(t) * \hat{h}(t)]|_{t=nT}$$
$$= \left(\int_{-\infty}^{\infty} p_T(\tau)\hat{h}(t - \tau)\, d\tau\right)\Bigg|_{t=nT} \tag{2}$$

where $p_T(t)$, impulse response of ZOH, is a pulse with width of p as shown in Fig. l(a), $\hat{h}(t)$ is the impulse response of the continuous-time loop filter, $h(n)$ is the impulse response of discrete-time loop, and $*$ denotes time convolution. Since $p_T(t)$ has a pulse waveform, (1) and (2) are known as the pulse invariant transformation.

A. NRZ Transformation

A NRZ, RZ (return-to-zero) and HZ (half-delay RZ) DAC waveforms represented by $R_{\mathrm{NZ}}(t), R_{\mathrm{RZ}}(t)$ and $R_{\mathrm{HZ}}(t)$ are shown in Fig. 2. Consider the case where $p = T$ corresponding to NRZ feedback. Then the loop filter NRZ pulse response from (2) can be described as follows:

$$h(t) = R_{\mathrm{NZ}}(t) * \hat{h}(t) = \int_{-\infty}^{\infty} R_{\mathrm{NZ}}(\tau)\hat{h}(t - \tau)\, d\tau$$
$$= \begin{cases} \displaystyle\int_0^t \hat{h}(t - \tau)\, d\tau & 0 \le t < T \\[2mm] \displaystyle\int_0^T \hat{h}(t - \tau)\, d\tau & t \ge T \\[2mm] 0 & t < 0. \end{cases} \tag{3}$$

For a continuous-time loop filter described in residue form by

$$\hat{H}(s) = \sum_{k=1}^{\mathbf{N}} \frac{\hat{a}_k}{s - s_k} \tag{4}$$

the impulse response would be

$$\hat{h}(t) = \sum_{k=1}^{\mathrm{N}} \hat{a}_k e^{s_k t} u(t).$$

Substituting $\hat{h}(t)$ into (3), it can be shown that the equivalent discrete-time loop filter is

$$H(z) = \sum_{k=1}^{N} \frac{a_k z^{-1}}{1 - z_k z^{-1}} \tag{5}$$

where the new residue is

$$a_k = \frac{a_k}{-s_k}(1 - e^{s_k T}) \tag{6}$$

and the new pole is at $z_k = e^{s_k T}$

This has the properties one would expect: a pole at $s = 0$ transforms to one at $z = 1$, and a pole at $s = j2\pi(f_s/4)$ transforms to one at $z = j$. Equations (4)–(6) give a simple translation that allows a designer to take an arbitrary $H(z)$, rewrite it in the form of (5), and get an $H(s)$ that gives an exact equivalent continuous-time loop. That's enough to design continuous-time bandpass (or lowpass, for that matter) $\Delta\Sigma$ converters, except for a couple of "fine points" that need to be addressed: (5) can't handle multiple poles such as those found in a conventional second-order $\Delta\Sigma$ modulator or its bandpass version; and high-linearity feedback DAC's use RZ waveforms rather than NRZ. Now we'll correct these problems.

B. Multiple-Pole System

Repeated poles in a rational function produce additional terms (besides those in (5)) in the partial fraction expansion, which have the form

$$\frac{a_k'}{(z - z_k)^2}. \tag{7}$$

The poles are moved to points s_k with $e^{s_k T} = z_k$, just as before, and the corresponding term in the continuous-time equivalent becomes

$$a_k' \frac{\dfrac{(1 - e^{-s_k T} - s_k T)}{(1 - e^{s_k T})^2}\dfrac{s}{T} + \dfrac{s_k^2}{(1 - e^{s_k T})^2}}{(s - s_k)^2} \tag{8}$$

which has repeated poles, just as in the x-domain, but has a numerator with both bandpass (s) and lowpass (constant) terms. From (4) to (8) it can easily be shown that a conventional second-order $\Delta\Sigma$ modulator with $H(z) = (2z - 1)/(z - 1)^2$ has a continuous-time equivalent $\hat{H}(s) = (1 + 1.5sT)/s^2T^2$ which has already been derived by a different method in [11]. For a complex pole the numerator in (8) has complex coefficients, but a conjugate term $a_k'/(z - \overline{z_k})^2$ produces a conjugate numerator term.

The particularly important case

$$H(z) = \frac{z^{-2}(2 + z^{-2})}{(1 + z^{-2})^2} \qquad (9)$$

which gives a fourth-order bandpass converter, for example, produces a fourth-order continuous-time filter with a third-order numerator and a double pole at $1/(4T) = f_s/4$: (see (10) at the bottom of the page).

C, RZ and HZ Transformation

A second generalization of (4)-(6) is needed to allow the use of return-to-zero (RZ) and half-delay return-to-zero DAC waveforms [8], [9] like the ones shown in Fig. 2. The effect this has is to change the integration (convolution) boundary in (3) from (for NRZ DAC) to [O,T/2] and $[T/2, T]$ for RZ and HZ DAC's, respectively.

In an RZ DAC the zero-order hold, $(1 - e^{-sT})/s$, is replaced with a half-sample hold, $(1 - \exp(-sT/2))/s$, which would just make a straightforward change in (6) for the single pole case

$$a_k = \frac{a_k}{-s_k}(1 - e^{s_k T/2})e^{s_k T/2}. \qquad (11)$$

Correspondingly in an HZ DAC the zero-order hold, $(1 - e^{-sT}/s)$, is replaced with a half delayed half-sample hold, $\exp(-sT/2)(1 - \exp(-sT/2))/s$, which would just need another straightforward change in (6) for the single pole case

$$a_k = \frac{a_k}{-s_k}(1 - e^{s_k T/2}). \qquad (12)$$

It can be shown that the RZ pulse transformation of the double-pole function given in *(7)* is shown in (13) at the bottom of the page, and its HZ pulse transformation is

$$a_k' e^{-s_k T/2} \frac{\dfrac{(1 - 0.5 s_k T - e^{-s_k T/2})}{(1 - e^{s_k T/2})^2}\dfrac{s}{T} + \dfrac{0.54}{(1 - e^{s_k T/2})^2}}{(s - s_k)^2} \qquad (14)$$

The multiple-pole transformation is actually an extension of the single-pole transformation. A multiple-pole function can be considered as a function with distinct poles in which the poles are hypothetically deviated slightly from each other. Then the single pole transformation (4)-(6) for NRZ and (1 1), (12) for RZ and HZ, respectively, can easily be applied on the partial fraction expansion form of the new hypothetically single-pole functions. In the second step in order to obtain the original multiple-pole function in the other domain (say s-domain) one may use L'Hopital's rule as many times as necessary $(n - 1$ times for a multiple-pole function of order n). In the last step the deviated poles should approach their original places in order to obtain the limit function value. The example of RZ and HZ double-pole transformations for z-domain to s-domain $(z2s)$ is given in [8], Appendix A].

These programs have been written in "Mathematica" [8]. From (11) and (13) it can be shown that the multiple-pole fourth-order system given in (9) has the RZ continuous-time filter (one-delay scheme) as follows in (15) at the bottom of the page.

In Table I, the corresponding NRZ and RZ continuous-time loop transfer functions for some conventional $\Delta\Sigma$ modulators have been shown.

The equivalent z-domain and s-domain modulators obtained from the preceding transformation have been simulated. Fig. 3 shows the simulated dynamic range of the fourth-order discrete-time and the NRZ equivalent continuous-time modulator in (10) as well as the second-order modulator given in Table I:

$$\hat{H}(s) = \frac{-\dfrac{\pi}{4T}s + \dfrac{1}{2}\left(\dfrac{\pi}{2T}\right)^2}{s^2 + \left(\dfrac{\pi}{2T}\right)^2}. \qquad (16)$$

The simulated SNR's in Fig. 3 for discrete and continuous-time modulators are quite close. For example, in a l-MHz bandwidth and for a 20-MHz sinusoidal input, the maximum

$$\hat{H}(s) = \frac{\left(\dfrac{\pi}{2} - \dfrac{1}{4}\right)\dfrac{s^3}{T} + \left(\dfrac{3\pi^2}{16} + \dfrac{\pi}{4}\right)\dfrac{s^2}{T^2} + \left(\dfrac{\pi^3}{8} + \dfrac{\pi^2}{16}\right)\dfrac{s}{T^3} + \dfrac{3}{4}\left(\dfrac{\pi}{2T}\right)^4}{\left(s^2 + \left(\dfrac{\pi}{2T}\right)^2\right)^2}. \qquad (10)$$

$$a_k' e^{-s_k T} \frac{\dfrac{(1 - e^{-s_k T/2} - s_k T(1 - 0.5 e^{-s_k T/2}))}{(1 - e^{s_k T/2})^2}\dfrac{s}{T} + \dfrac{s_k^2(1 - 0.5 e^{-s_k T/2})}{(1 - e^{s_k T/2})^2}}{(s - s_k)^2} \qquad (13)$$

$$\hat{H}(s) = \frac{\dfrac{9.4142\pi - 9.65685}{16}\dfrac{s^3}{T} + \dfrac{7.24264\pi^2 + 4\pi}{16}\dfrac{s^2}{T^2} + \dfrac{2.35355\pi^3 + 2.41421\pi^2}{16}\dfrac{s}{T^3} + 1.81066\left(\dfrac{\pi}{2T}\right)^4}{\left(s^2 + \left(\dfrac{\pi}{2T}\right)^2\right)^2}. \qquad (15)$$

TABLE I
EXAMPLES OF s- AND z-DOMAIN $\Delta\Sigma$ MODULATOR LOOP TRANSFER FUNCTIONS

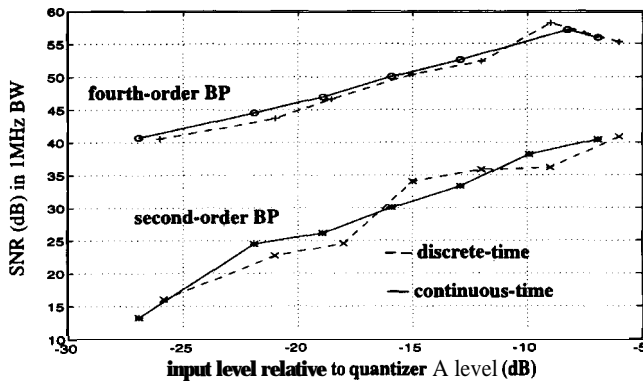| Sigma-Delta Modulators	First Order Lowpass	Second Order Lowpass	Second Order Bandpass (one resonator at $\pi/2T$)	Second Order Bandpass (one resonator at $\pi/2T$), with one digital delay in the s-domain loop	General Second Order Bandpass (one resonator at θ/T)
$H(z)$	$-\dfrac{z^{-1}}{1-z^{-1}}$	$-\dfrac{z^{-1}(2-z^{-1})}{(1-z^{-1})^2}$	$\dfrac{z^{-2}}{1+z^{-2}}$	$z^{-1}\cdot\dfrac{z^{-1}}{1+z^{-2}}$	$\dfrac{z^{-1}(2\cos\theta-z^{-1})}{1-2\cos\theta z^{-1}+z^{-2}}$
NRZ $\hat{H}(s)$	$-\dfrac{1}{Ts}$	$-\dfrac{1+1.5Ts}{T^2s^2}$	$\dfrac{-\frac{\pi}{4T}s+\frac{1}{2}\left(\frac{\pi}{2T}\right)^2}{s^2+\left(\frac{\pi}{2T}\right)^2}$	$\dfrac{\frac{\pi}{4T}s+\frac{1}{2}\left(\frac{\pi}{2T}\right)^2}{s^2+\left(\frac{\pi}{2T}\right)^2}$	$\dfrac{\frac{\theta}{T}\cdot\frac{\cos2\theta-\cos\theta}{2\sin\theta(1-\cos\theta)}s-\frac{\theta^2}{T^2}\cdot\frac{\sin2\theta-\sin\theta}{2\sin\theta(1-\cos\theta)}}{s^2+\frac{\theta^2}{T^2}}$
RZ $\hat{H}(s)$	$-\dfrac{2}{Ts}$	$-\dfrac{2+2.5Ts}{T^2s^2}$	$\dfrac{-\frac{2.414\pi}{4T}s+\frac{1}{2}\left(\frac{\pi}{2T}\right)^2}{s^2+\left(\frac{\pi}{2T}\right)^2}$	$\dfrac{-\frac{\pi}{4T}s+\frac{2.414}{2}\left(\frac{\pi}{2T}\right)^2}{s^2+\left(\frac{\pi}{2T}\right)^2}$	$\dfrac{\frac{\theta}{T}\cdot\frac{\cos\frac{3\theta}{2}-\cos\theta}{2\sin\theta\left(1-\cos\frac{\theta}{2}\right)}s-\frac{\theta^2}{T^2}\cdot\frac{\sin\frac{3\theta}{2}-\sin\theta}{2\sin\theta\left(1-\cos\frac{\theta}{2}\right)}}{s^2+\frac{\theta^2}{T^2}}$

Fig. 3. Simulation results of discrete-time and continuous-time modulators derived by the pulse invariant transformation for fourth- and second-order modulators ($f_{\text{in}}=20$ MHz and BW $=1$ MHz).

SNR's for the fourth-order bandpass discrete and continuous-time (10) modulators were 55.25 and 55.93 dB, respectively, and 41.68 dB and 40.48 dB for the second-order system. It should be noted that because the in-band signal gain is (0 dB) for discrete-time modulators but almost 1 **.11** (0.9 dB) for the second- and fourth-order continuous-time modulators (explained in Section III), the input levels were chosen accordingly (-6 dB in discrete-time and -6.9 dB in continuous-time) for the maximum input levels, as shown in Fig. 3. This gain difference, combined with numerical errors in simulation, is enough to explain the minor differences in SNR observed in simulations.

As mentioned, the loop transfer function for the continuous-time modulator is inherently discrete-time. This is due to the presence of the sampler inside the loop as shown in Fig. 1. Therefore, one can implement different equivalent continuous-time modulators depending on the number of delays chosen in the digital side of the loop preceding the DAC and after the comparator. For instance, as shown in Table I, the open loop transfer function of a second-order bandpass modulator is $H(z)=z^{-2}/1+z^{-2}$. One way to implement the continuous-time loop is to apply the pulse invariant transformation on $H(z)$ (having no digital delay inside the loop) which gives a continuous-time loop filter with a RHP zero as shown in column 4 of Table I and graphically in Fig. 4. The other way is to have one delay in the digital side of the loop and to apply the pulse invariant transformation on the remaining part of $H(z)$, *i.e.* $z^{-1}/(1+z^{-2})$, which gives a continuous-time loop filter with a LHP zero as shown in column 5 of Table I and graphically in Fig. 4. It should be noted that in the pulse invariant transformation a z^{-1} is present in the numerator of each partial fraction as shown in (5). Thus in order to derive a continuous-time loop filter we need to keep at least one delay (z^{-1}) in the numerator to ensure causality. This determines the number of possible ways to implement the equivalent continuous-time modulators from a discrete-time modulator. Obviously, for the second and fourth-order bandpass modulators there are two different ways to implement the continuous-time loop: the zero-delay and one-delay schemes. The fourth-order continuous-time filter defined by (10) is based on the one-delay scheme. Both transformation schemes for this fourth-order modulator are graphically illustrated in Fig. 5.

III. IMPLICIT ANTI-ALIAS (IMAGE) FILTERING

In [11] it was shown that a lowpass continuous-time $\Delta\Sigma$ modulator provides an inherent anti-alias filtering on the input signal path. In the continuous-time lowpass case, the signal transfer function contains a "sinc" term. Since its zeros are located at integer multiples of the sampling frequency (f_s), clock-image signals are attenuated significantly which otherwise would be aliased into the desired frequency band. We will generalize this observation to the bandpass $\Delta\Sigma$ modulator in this section.
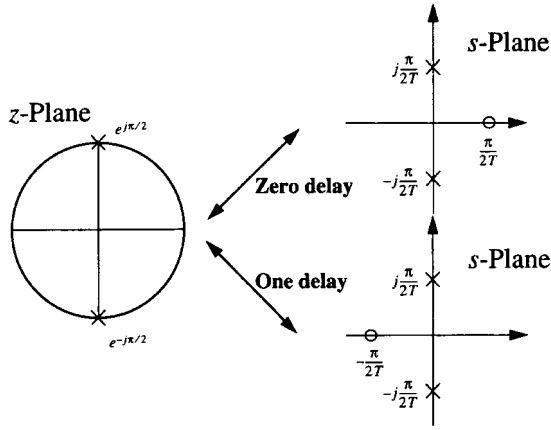
Fig. 4. Pole-zero mapping between continuous-time and discrete-time loop filters in a second-order loop.
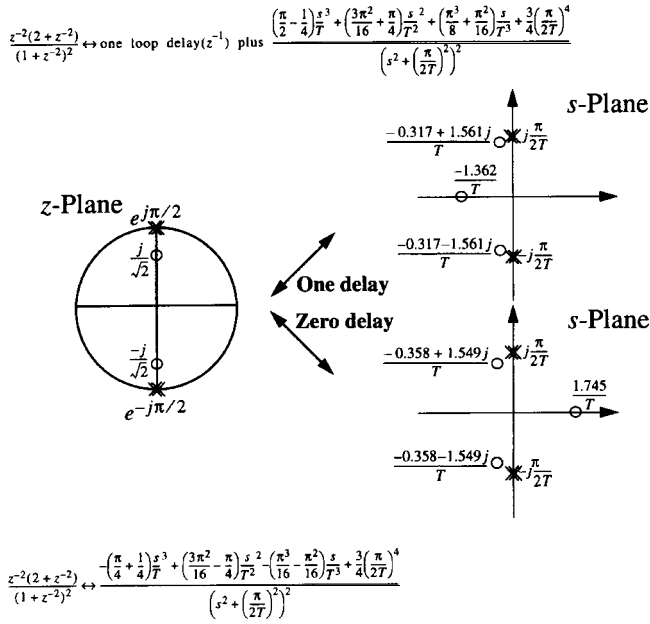
$$\frac{z^{-2}(2+z^{-2})}{(1+z^{-2})^2} \leftrightarrow \text{one loop delay}(z^{-1}) \text{ plus } \frac{\left(\frac{\pi}{2}-\frac{1}{4}\right)\frac{s^3}{T}+\left(\frac{3\pi^2}{16}+\frac{\pi}{4}\right)\frac{s^2}{T^2}+\left(\frac{\pi^3}{8}+\frac{\pi^2}{16}\right)\frac{s}{T^3}+\frac{3}{4}\left(\frac{\pi}{2T}\right)^4}{\left(s^2+\left(\frac{\pi}{2T}\right)^2\right)^2}$$

$$\frac{z^{-2}(2+z^{-2})}{(1+z^{-2})^2} \leftrightarrow \frac{-\left(\frac{\pi}{4}+\frac{1}{4}\right)\frac{s^3}{T}+\left(\frac{3\pi^2}{16}-\frac{\pi}{4}\right)\frac{s^2}{T^2}-\left(\frac{\pi^3}{16}-\frac{\pi^2}{16}\right)\frac{s}{T^3}+\frac{3}{4}\left(\frac{\pi}{2T}\right)^4}{\left(s^2+\left(\frac{\pi}{2T}\right)^2\right)^2}$$

Fig. 5. Pole-zero mapping between continuous-time and discrete-time loop filters in a fourth-order loop.

Fig. 6(a) shows another representation of the continuous-time modulator shown in Fig. 1. The quantizer is replaced by its linear additive noise model e(k). Moreover, the continuous-time filter, $\hat{H}(s)$, and sampler are moved to the input side of the input summer, which obviously doesn't change the input or loop transfer function. Any additional anti-alias filter preceding the $\Delta\Sigma$ modulator can be included in the $\Delta\Sigma$ modulator prefilter $\hat{H}(s)$ generalizing it to some $\hat{G}(s)$ as shown in Fig. 6. For the purpose of this paper we assume $\hat{G}(s)=\hat{H}(s)$. As explained in Section II, the loop transfer function is

$$H(z) = Z\left[\frac{1-e^{-sp}}{s}\hat{H}(s)\right].$$

Therefore, the noise transfer function $(\mathrm{NTF}(z))$ in Fig. 6(a) is

$$\mathrm{NTF}(z) = \frac{Y(z)}{U_1(z)} = \frac{1}{1-H(z)}. \qquad (17)$$

We know that the signal transfer function of the equivalent discrete-time modulator is $H(z)/1-H(z)$, so as shown in Fig. 6(b) and (c) the frequency response of the filter that should be placed in cascade with the input of the discrete-time modulator in order to make its response identical to that of the continuous-time version is

$$F_{aa}(\omega) = \frac{\hat{G}(j\omega)}{H(e^{j\omega T})} = \frac{\hat{G}(j\omega)}{H(e^{j\omega T})}. \qquad (18)$$

It should be noted that because there is a sampler on the signal path, the input signals which are located out of the signal band region of $-\pi/T < \omega < \pi/T$ **are** aliased into the in-band. However, as will be seen the out of band signals, especially the images of the clock frequency are attenuated significantly. For example, for the second-order bandpass case given in (16) and Table I, we have $H(z) = z^{-2}/1+z^{-2}$ and so from (18)

$$|F_{aa}(\omega)| = \frac{\left|\frac{-\pi}{4T}j\omega + \frac{1}{2}\left(\frac{\pi}{2T}\right)^2\right|}{\left|(j\omega)^2+\left(\frac{\pi}{2T}\right)^2\right|} \cdot \left|\frac{1+e^{-2j\omega T}}{e^{-2j\omega T}}\right|$$

$$= \frac{2\cos(\omega T)\left[\left(\frac{\pi}{2\sqrt{2}T}\right)^4 + \left(\frac{\pi}{4T}\omega\right)^2\right]^{1/2}}{\left(\frac{\pi}{2T}\right)^2 - \omega^2}. \qquad (19)$$

The zeros of the implicit anti-alias filter given in (19) are the same as zeros of $\cos(\omega T)$ at $w = 2n\pi/T \pm \pi/(2T)$ or at $f = nf_s \pm f_o$ where, $n = \pm 1, \pm 2, \pm 3, \cdots$ and $f_o = f_s/4$ (in this example). These are "image frequencies" at which, in a pure discrete-time system, input signals would alias into the band of interest. The attenuation $F_{aa}(\omega)$ provides at image frequencies (which is where its zeros are) is desirable for the overall system. The numerator of (19) also has a zero at $n = 0$ $(\omega = \pi/(2T))$, which is in the desired band, but this is cancelled by a denominator zero $(\omega^2 - (\pi/(2T))^2)$. L'Hpital's rule can be used to resolve the O/O ambiguity and shows that $|F_{aa}(\omega = \pi/2T)| = \pi/(2\sqrt{2})$. This cancellation of zeros at f_o is a mathematical artifact, and doesn't affect stability.

The $F_{aa}(\omega)$ for three different modulators are shown in Fig. 7: one is the second-order case, one a fourth-order with $\hat{G}(s) = \hat{H}(s)$ given in (10), and one a fourth-order with its input arranged so that

$$\hat{G}(s) = 0.25\frac{\left(\frac{\pi}{2}-1\right)\frac{s^3}{T} - \pi\frac{s^2}{T^2} + \left(\frac{\pi}{2}+1\right)\left(\frac{\pi}{2}\right)^2\frac{s}{T^3}}{\left(s^2+\left(\frac{\pi}{2T}\right)^2\right)^2}.$$

$$(20)$$

The latter provides a zero at $s = 0$ as explained in [7].

For the second-order bandpass modulator, from (19) we showed that the zeros of the implicit anti-alias frequency response of the continuous-time $\Delta\Sigma$ modulator are at $f = nf_s \pm f_o$, however, this conclusion could be easily generalized to any continuous-time $\Delta\Sigma$ modulator (bandpass or lowpass) derived by the pulse invariant transformation explained in
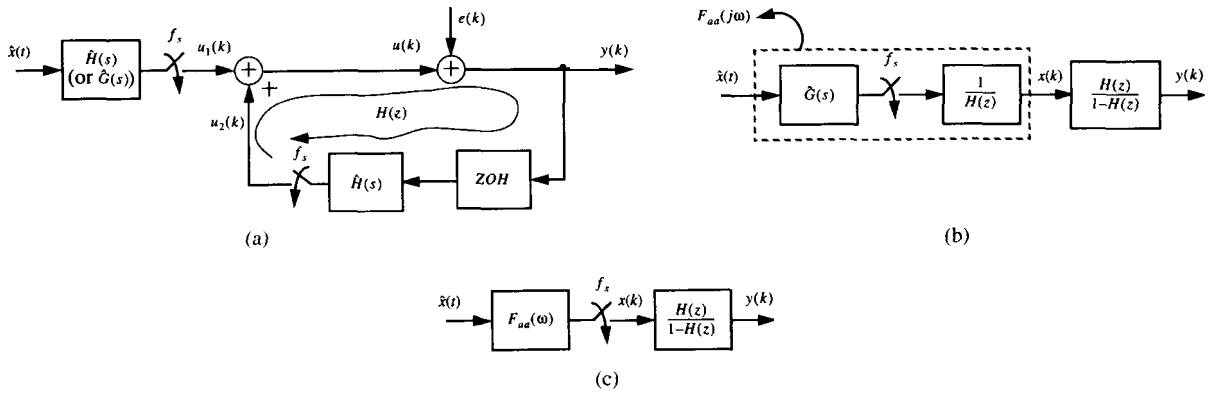
Fig. 6. (a) One representation of a continuous-time modulator, (b) Another arrangement of (a). (c) The equivalent discrete-time modulator with an extra input filter shown by $F_{aa}(\omega)$.
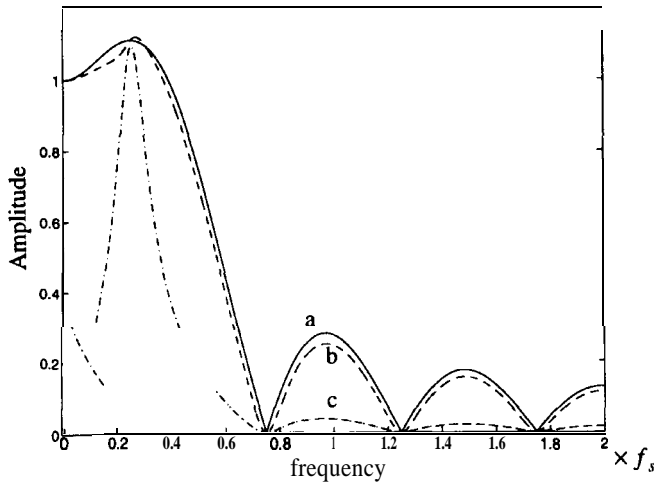

Fig. 7. Implicit antialias filter frequency response in (a) a second-order (solid line). (b) A fourth-order $(\hat{G}(s) = H(s))$ (dashed line). (c) A fourth-order with an optimized $\hat{G}(s)\Delta\Sigma$ modulators (dashed-dot line) (resonator at $f = f_s/4$).

Section II. As (18) shows the anti-alias frequency response is the product of the feedforward frequency response represented by $\hat{G}(j\omega)$ (in Fig. 6) and the inverse of the discrete-time loop frequency response $1/H(e^{j\omega T})$. The resonance (pole) frequency of $\hat{G}(j\omega)$ is at $f = f_0$ and the first notch of the noise transfer function is at $f = f_0$ too, so the value of signal frequency response at f_o is O/O which after resolving the ambiguity yields a finite value (like $\pi/2\sqrt{2} \approx 1.11$ for the second-order bandpass case).

The feedforward frequency response, $\hat{G}(j\omega)$ doesn't have a zero on the $j\omega$ axis (except in a bandpass modulator which could have a zero at DC as shown in Fig. 7(c) and [7]). Thus, the zeros of signal frequency response are determined by the remaining zeros of the noise transfer function, which obviously are at $f = nf_s \pm f_o, n = \pm 1, \pm 2, \pm 3, \cdots$ as obtained for the second-order example. It should be noted that for a lowpass continuous time modulator the resonance frequency is at $f_o = 0$ (we have an integrator instead of resonator), so according to the preceding derivation the zeros of signal frequency response are at $f = nf_s, n = \pm 1, \pm 2, \pm 3, \cdots$ which is consistent with [11]. Therefore continuous-time $\Delta\Sigma$ modulator compared to discrete-time (switched-C) modulator has the advantage that

it provides a free anti-alias filtering to reduce the spurious images of the clock frequency significantly.

All this shows that the difference between a continuous-time and a discrete-time modulator having equivalent loop functions is in their signal transfer functions. A continuous-time $\Delta\Sigma$ modulator can be modeled by a system including a "free" anti-alias filter with a frequency response given in (18) followed by a sampler and its equivalent discrete-time modulator.

IV. SECOND-ORDER Gm-C MODULATOR WITH TUNING

We used a Gm-C biquad filter chip [12] tuned at a frequency (f_o) between 40 MHz to 70 MHz with a built-in latched comparator to make an experimental $\Delta\Sigma$ loop nominally clocked at $4 f_o$, i.e., with f_s in the 160 MHz-280 MHz range. A second filter chip was utilized as the voltage-controlled oscillator (VCO) in a PLL to implement the master-slave tuning scheme. The biquad filters were implemented in a 0.8 μm BiCMOS process.

A. Modulator Implementation

A block diagram of the modulator including the tuning circuitry is shown in Fig. 8(a). The tuning scheme is discussed in Section IV-B. The dashed lines in Fig. 8(a) enclose the chips used, while the additional blocks in the figure are discrete components. The biquad filter chip was fully differential and consisted of five transconductor blocks. For simplicity the single-ended block level schematic of the filter is shown in Fig. 8(b) where the g_m terms represent the biquad transconductors. Further details on the biquad can be found in [12]. The comparator output is fed to a variable attenuator [represented by k in Fig. 8(a)] whose output is added to the input signal by a passive combiner network. The attenuator is used to adjust the sensitivity of the $\Delta\Sigma$ A/D and to increase its linearity while keeping the dynamic range unchanged (within limits).

It can be shown that the transfer function of the filter in Fig. 8(b) (shown in (21) at the bottom of the next page) where the g_o terms represent transconductor output conductances. The transconductor terms represented by g_{mx} and $-g_{mf}$ in Fig. 8(b) are used to tune the poles of filter as can be inferred from the constant term in the denominator of (21). For example, at 50 MHz ω_o is $2\pi(50)$ Mrad/s The transconductor
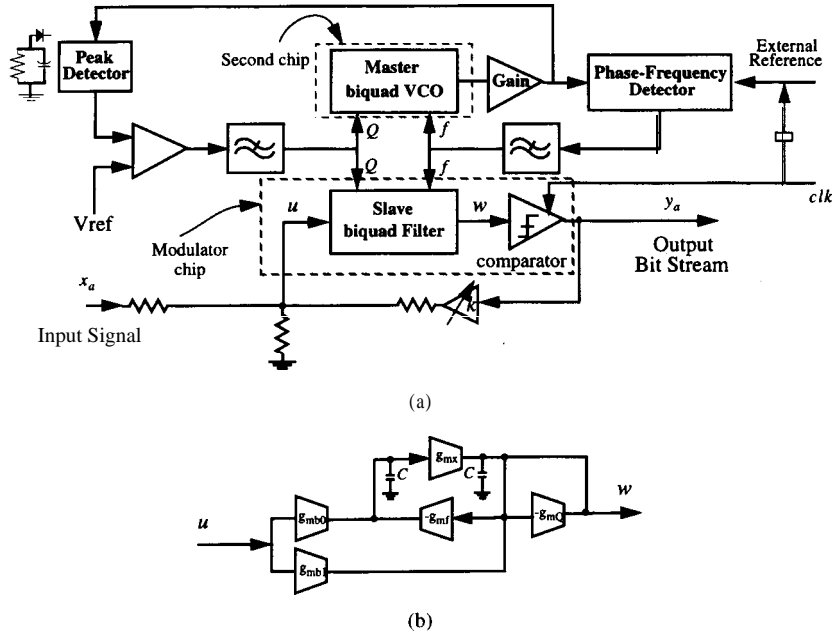
Fig. 8.   Single ended diagram of (a) the second-order $\Sigma\Delta$ modulator with tuning circuitry. (b) Gm-C biquad filter.

represented by $-g_{mQ}$ is set negative, cancelling out the effect of transconductors' output resistance in the s coefficient in the denominator of (21), in order to provide infinite Q poles as required for the second-order transfer function in (16). The transconductor terms in the branches represented by g_{mb0} and g_{mb1} in Fig. 8(b) should be tuned to set the required zero for the loop transfer function. It can be shown that if $g_{mx} = g_{mf} = g_m$ then we should have $g_{mb0} = -g_{mb1} = 0.5g_m$ in order to make filter's zero given in (21) the same as the ideal transfer function's zero given in (16). However, as (21) shows, there will be some errors in zero location due to the finite transconductors' output resistance $(1/g_o$ values). This error doesn't lead to modulator instability as the second-order bandpass $\Delta\Sigma$ modulator is a robust system, however it reduces the maximum achievable SNR.

B. Automatic Tuning

Continuous-time filters are subject to fabrication tolerances, temperature variations and parasitic effects, hence tuning is required especially at high speed. To correct the transfer function, a tuning circuit was implemented. The master-slave tuning scheme is commonly used for frequency and Q-tuning of a main filter (slave). The resonance frequency of the master voltage-controlled filter (VCF) [13], or the master voltage-controlled oscillator (VCO) [14], [15] is locked to an external accurate frequency by a PLL system. The Q of the master VCF or VCO can be controlled by comparing the amplitude of the master output signal to a reference voltage. The main

filter (slave) is tuned by the same frequency and Q control voltages of the master.

For tuning the $\Delta\Sigma$ modulator loop filter, a master-slave scheme was implemented as shown in Fig. 8(a). The ideal second-order bandpass $\Delta\Sigma$ loop transfer function in (16) represents an infinite Q filter with two poles on the $j\omega$ axis as shown in Fig. 4(a). Notice that this transfer function can be regarded as a typical oscillator. Therefore, the VCO master-slave tuning scheme is naturally suited for our purpose. It should be noted that unlike traditional master-slave schemes which tune an open-loop slave filter, the slave filter in our continuous-time $\Delta\Sigma$ modulator is working in closed-loop. As will be shown in Section V, tuning of the open loop master resonance frequency (VCO) will result in the tuning of the $\Delta\Sigma$ loop resonance frequency and therefore the tuning of the bandpass $\Delta\Sigma$ noise transfer function (NTF) notch frequency. The Q of the filters was tuned by comparing the amplitude of the VCO output signal with a reference voltage. The amplitude of the VCO output signal was detected by a Schottky-diode peak-detector as shown in Fig. 8(a).

The tunablity of a continuous-time bandpass $\Delta\Sigma$ converter center frequency with its inherent anti-alias filtering can be advantageous over a bandpass switched-C $\Delta\Sigma$ converter and could provide a new approach for channel selection in digital radio receivers. The idea is shown in Fig. 9. Having a tunable bandpass $\Delta\Sigma$ converter at the IF stage removes the necessity of channel selection at the RF. So, as illustrated in Fig. 9, one may use a fixed local oscillator (presumably a SAW or

$$\frac{W}{U} = \frac{\dfrac{g_{mb1}}{c}s + \dfrac{g_{mb0}g_{mx} + g_{mb1}(g_{of} + g_{ob0})}{C^2}}{s^2 + \left(\dfrac{g_{of} + g_{ob0} + g_{ox} + g_{ob1} + g_{oQ} - g_{mQ}}{C}\right)s + \dfrac{g_{mx}g_{mf} + (g_{of} + g_{ob0})(g_{ox} + g_{ob1} + g_{oQ} - g_{mQ})}{C^2}} \tag{21}$$
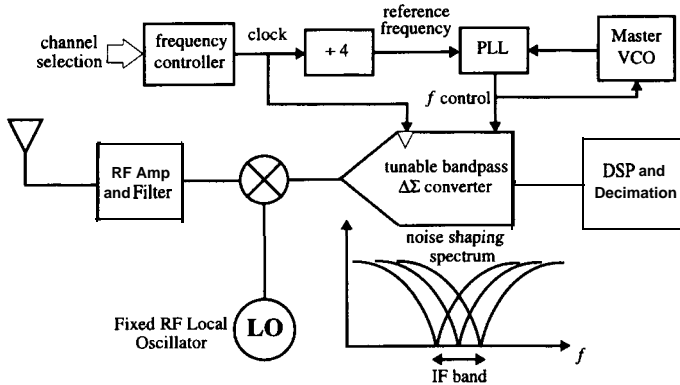
Fig. 9.   Block diagram showing the possible channel selection at the IF stage by a tunable bandpass $\Delta\Sigma$ modulator.

Fig. 10. Measured SNR versus input signal level for different attenuation values $(k_1 = k_2 - 10$ **dB**$)$, for BW = 200 KHZ.

Fig. 11.   Experimental output spectra of the second-order modulator.

crystal oscillator) and move the synthesizer to the IF stage which would consume less power as it would operate at lower frequency. Since the $\Delta\Sigma$ master-slave tuning scheme shown in Fig. 8(a) uses a PLL, the only requirement for channel selection at the IF is a frequency controller as shown in Fig. 9.

It should be noted that because the $\Delta\Sigma$ modulator center frequency in this example is one quarter of the clock frequency ($\Delta\Sigma$ NTF zeros are at $\pm j$ as shown in Fig. 4(a)), by changing the reference frequency the clock frequency should be changed accordingly. This relationship is shown in Fig. 8(a) by the dotted line connection between the clock and the external reference signal and by the frequency divider (by 4) as shown in Fig. 9.

V. EXPERIMENTAL RESULTS

A. Signal-to-Noise Ratio (SNR)

The SNR obtained is plotted against the input signal power in Fig. 10 for two different loop attenuation (k) values. The input signal was a 50 MHz sinusoid and the clock frequency was 200 MHz. The output digital data was supplied to a logic analyzer. The plots shown in Fig. 10 were obtained by taking a 2^{18}-point Hanning windowed FFT of the $\Delta\Sigma$ bit stream for each input signal level. As can be seen from Fig. 10 the maximum SNR in a 200 KHz bandwidth is 46 dB, and occurs for input level of $P_{in} = -17$ dBm with $k = k_1$. By reducing the attenuation the same SNR was achieved at $P_{in} = -6$ dBm (for $k = k_2$), where $k_2 - k_1 = 10$ dB.

The noise shaping spectrum obtained by taking an FFT (using a Hanning window) of the 200 MHz $\Delta\Sigma$ modulator output bit stream for a sinusoidal input signal of $P_{in} = -17$ dBm with $k = k_1$ is plotted in Fig. 11. It should be noted that the signal transfer function from input to output provides 13 dB and 0 dB gain for $k = k_1$ and $k = k_2$, respectively, which is not shown in Figs. 10 and 11.

B. Linearity

Analog-to-digital conversion at the IF (or RF) stage for digital radio receivers puts linearity constraints on the bandpass A/D converter. The linearity of the $\Delta\Sigma$ modulator is limited by the linearity of the filter inside the loop which
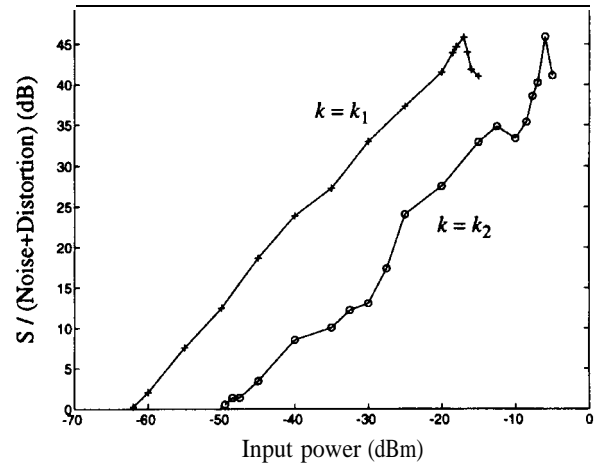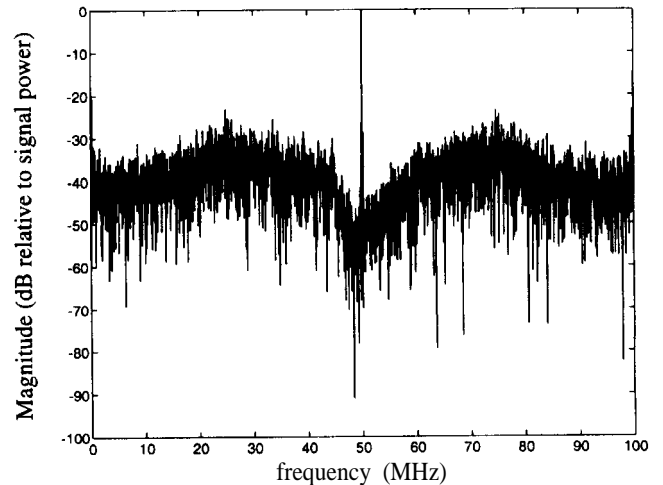
in our case is a Gm-C filter. Fig. 10 shows that for higher quantization gain (lower loop attenuation $k = k_2$), the second-order $\Delta\Sigma$ modulator presents higher integral and differential nonlinearity. Although $\Delta\Sigma$ A/D converters are considered to be highly linear A/D's, in low order $\Delta\Sigma$ modulators (first-order lowpass and second-order bandpass), the noise and distortion depend on the signal level [16] and also on signal frequency in the second-order bandpass $\Delta\Sigma$ modulator, so causing more nonlinearity. As the SNR plot for higher loop attenuation $(k = k_1)$ in Fig. 10 shows this nonlinearity (noise dependency on signal level) was overcome significantly by reducing the loop gain.

Another important linearity measure in A/D converters is the third-order intermodulation product (IM3). Fig. 12 shows a plot of IM3 level against the input signal level (for $k = k_1$). Two in-band tones at equal power levels with a 50 KHz separation were applied to the modulator and the IM3 products were obtained by taking a 2^{18}-point FFT of the $\Delta\Sigma$ bit stream. Although IM3 products for a 0 dB total input signal power (relative to the input overload point) are 21 dB below the output tone levels, at -3.5 dB total input power the IM3
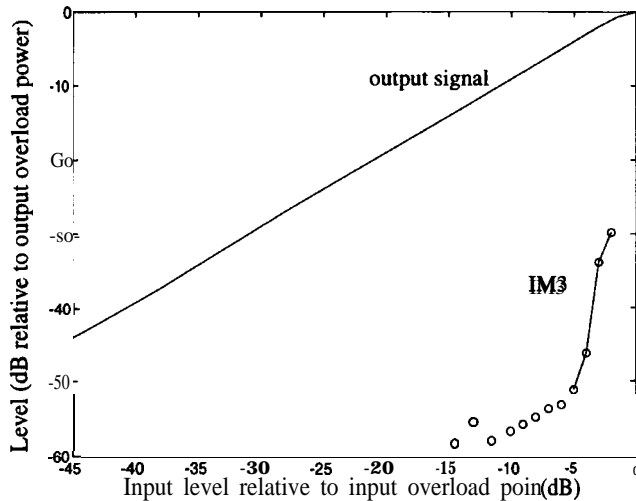
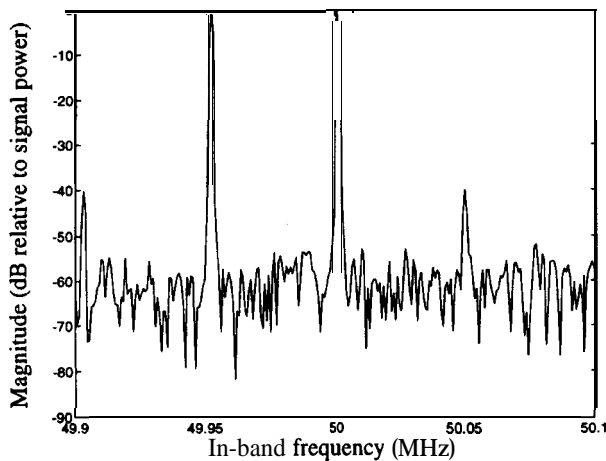Fig, 12. Measured output signal and IM3 level versus the input signal level.

TABLE II
THE MEASURED IMPLICIT ANTI-ALIAS FILTER FREQUENCY RESPONSE

f_{in} (MHz)	aliased frequency (MHz)	attenuation (dB)
149.6	50.4	34
149.8	50.2	39
150	50	42
150.2	49.8	39
150.4	49.6	34
249.6	49.6	39
250	50	49
250.4	50.4	45

Fig. 13. Intermodulation (linearity) performance of $\Delta\Sigma$ modulator with two in-band input tones having -3.5 dB total power relative to overload point.
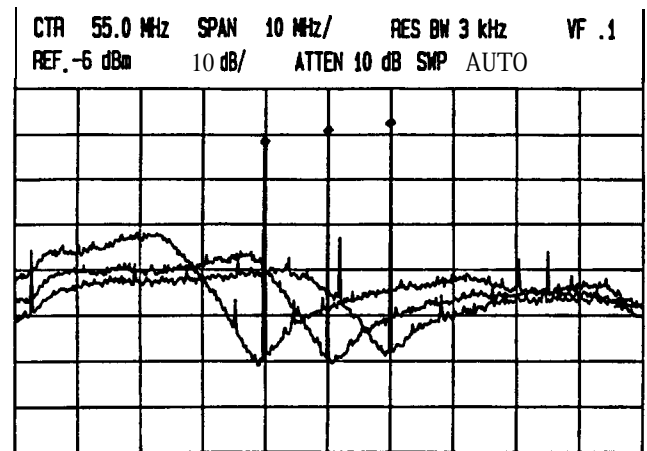
Fig, 14. Experimental result for tuning of the $\Delta\Sigma$ modulator noise-shaping center frequency. The three different tuned $\Delta\Sigma$ NTF notch frequencies are at 45, 55, and 65 MHz, respectively.

products drop to 40 dB below the output tone level, giving 1% distortion. Fig. 13 shows the performance of the $\Delta\Sigma$ modulator when two input tones at a -3.5 dB level (relative to overload) are supplied. For signal levels lower than -15 dB, IM3 levels are buried in the noise floor, so no in-band intermodulation was observed. Third-order intermodulation here is bigger than what was reported in [5]. The reason is attributed to the fact that the on-chip Gm-C resonators used here are more nonlinear than the discrete off-chip LC components used in [5].

C, Anti-Alias (Image) Performance

Table II lists the attenuation of the signals aliased into the in-band region (50 MHz) for various frequencies in the first (150 MHz) and second image frequency (250 MHz) bands. The level of aliased in-band signals at the higher and lower frequencies of images increase which demonstrates that the zeros of signal frequency response are at the image frequencies $(f = nf_s \pm f_o, n = \pm 1, \pm 2, \pm 3, \cdots)$ as was shown theoretically in Section III.

D. $\Delta\Sigma$ NTF Notch Frequency Control

As explained in Section IV-B and illustrated in Fig. 8(a), by changing the external reference frequency it was possible to change the bandpass $\Delta\Sigma$ NTF notch frequency using the master-slave tuning scheme.

Fig. 14 shows the experimental results of the $\Delta\Sigma$ NTF zeros (notches) tuned to three different frequencies (45, 55, and 65 MHz). The $\Delta\Sigma$ NTF notch frequency has been tuned between 40 MHz and 67.5 MHz providing a practical 50% tuning range. The Gm-C bandpass filter is tunable over the range of 10 MHz to 100 MHz [12]. however, at low frequencies its high-Q performance degrades. As shown in [7] and [8] for getting the maximum achievable SNR, the typical Q required for a bandpass $\Delta\Sigma$ modulator is at least 50. Therefore, the low frequency limit of the $\Delta\Sigma$ tuning range is due to the low Q performance of the Gm-C filter (at frequencies lower than 40 MHz). The high frequency limit of the $\Delta\Sigma$ tuning range is due to the frequency limitation of the off-chip phase-frequency detector used (Fig. 8(a)).

As expected a frequency mismatch was observed between the master VCO (external reference) and the slave $\Delta\Sigma$. The frequency offset between the external reference (master VCO frequency) and the $\Delta\Sigma$ NTF notch frequency (slave resonance frequency) over entire tuning band was almost fixed at 6.5 MHz. For example, for $\Delta\Sigma$ center frequencies at 45, 55, and 65 MHz shown in Fig. 14 the corresponding external reference frequencies were 38.5, 48.5, and 58.5 MHz, respectively. Although the master-slave tuning scheme is prone to mismatch between the master and the slave filters, this offset can be reduced significantly by using careful design and layout techniques and by placing both the master and slave filters on a single chip.

VI. CONCLUSION

The design of a continuous-time (bandpass or lowpass) $\Delta\Sigma$ modulator has been discussed. It has been shown that the pulse invariant transformation matches the time domain response of a continuous-time $\Delta\Sigma$ modulator loop to that of a discrete-time $\Delta\Sigma M$ equivalent. It has been shown that the continuous-time $\Delta\Sigma$ modulator contains an implicit anti-alias filtering in comparison to the discrete-time (switched-C) modulator, which is a significant advantage for bandpass A/D conversion.
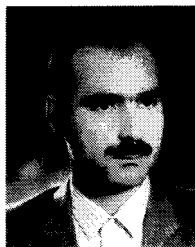
A second-order Gm-C $\Delta\Sigma$ prototype tuned by a master-slave tuning scheme has been demonstrated. The property of anti-alias (clock-image rejection) of this prototype $\Delta\Sigma$ was consistent with the theory. In terms of nonidealities, the filter (transconductor) nonlinearity and mismatching between master and slave filters were discussed. A more linear filter can be developed to achieve higher dynamic range along with lower intermodulation products. Integrating both master and slave on the same die would reduce the effect of frequency offset as well.

REFERENCES

[1] R. Schreier and M. Snelgrove, "Bandpass sigma-delta modulation," Electron. Lett., vol. 25 pp. 1560–1561 Nov. 1989.
[2] S. A. Jantzi, M. Snelgrove, and P. F. Ferguson, Jr., "A 4th-order bandpass sigma-delta modulator," in Proc. CICC, May 1992, pp. 16.5.1–4.
[3] F. W. Singor and M. Snelgrove, "10.7 MHz bandpass delta-sigma A/D modulatory' in Proc. CICC, May 1994, pp. 8.3.1–4.
[4] Gailus et al, "Method and arrangement for a sigma delta converter for bandpass signals," US. Patent 4857928, Aug. 1989.
[5] A. M. Thurston, T. H. Pearce, and M. J. Hawksford, "Bandpass implementation of the sigma-delta A-D conversion technique," in Proc. IEE Int. Conf. Analogue-to-Digital and Digital-to-Analogue Conversion, Swansea, U.K., Sept. 17–19, 1991, pp. 81–86.
[6] G. Troster, H. J. Dreler, H. J. Golberg, W. Schardein, E. Zocher, A. Wedel, K. Schoppe, and J. Arndt, "An interpolative bandpass converter on a 1.2-μm BiCMOS analog/digital array," IEEE J. Solid-State Circuits, vol. 28, pp. 471–476, Apr. 1993.
[7] O. Shoaei and W. M. Snelgrove, "Optimal (bandpass) continuous-time $\Sigma\Delta$ modulator," in Proc. ISCAS, May 30–June 2, 1994, vol. 5, pp. 489–492.
[8] O. Shoaei, "Continuous-time delta-sigma A/D converters for high-speed applications," Ph.D. dissertation, Carleton Univ., Ottawa, Ont., Canada, Feb. 1996.
[9] O. Shoaei and W. M. Snelgrove, "A multi-feedback design for LC bandpass delta-sigma modulators," in Proc. ISCAS, Apr. 29–May 3 1995, vol. 1, pp. 171-174.
[10] B. P, D. Signore, D. A. Kerth, N. S. Sooch and E. J. Swanson, "A monolithic 20.b delta-sigma A/D converter," IEEE J. Salid-State Circuits, vol. 25, pp. 1311-1316, Dec. 1990.
[11] C. Candy, "A use of double integration in sigma delta modulation," IEEE Trans. Commun., vol. COM-33, pp. 249-258, Mar. 1985.
[12] A. Shoval, W. M. Snelgrove, and D. A. Johns, "Adaptive pulse-shaping filter," IEEE J. Select. Areas Commun., vol. 13, pp. 1692-1702, Dec. 1995.
[13] V. Gopinathan, Y. P. Tsividis, K. S. Tan, and R. K. Hester, "Design considerations for high-frequency continuous-time filters and implementation of an antialiasing filter for digital video," IEEE J. Solid-State Circuits vol. 25, Dec. 1990.
[14] B. Nauta, "A CMOS transconductance-C filter technique for very high frequencies," IEEE J. Solid-State Circuits, vol. 27, Feb. 1992.
[15] J. M. Khoury, "Design of a 15-MHz CMOS continuous-time filter with on-chip tuning," IEEE J. Solid-State Circuits, vol. 26, Dec. 1991.
[16] J. C. Candy and G. C. Temes, Oversampling Delta-Sigma Data Converters. New York: IEEE, 1992, Introduction.

Omid Shoaei (M'96) received the B.Sc. and M.A.Sc. degrees from the University of Tehran, Iran, in 1986 and 1989, respectively, and the Ph.D. degree from Carleton University, Ottawa, Ont., Canada, in 1996, all in electrical engineering.

From 1994 to 1995 he was with BNR/NORTEL, Ottawa, as an intern student working towards the Ph.D. degree on high-speed Delta-Sigma modulators. In 1995 he was with Philsar Electronics Inc., Ottawa, working on the design of a bandpass Delta-Sigma data converter. Since December 1995, he has been a Member of Technical Staff with Lucent Technologies (formerly AT&T Bell Laboratories), Allentown, PA, where he is involved in the design of mixed analog/digital integrated circuit for LAN and fast ethernet systems.

W. Martin Snelgrove (M'81) received the B.A.Sc. degree in chemical engineering and the M.A.Sc. and Ph.D. degrees in electrical engineering, all from the University of Toronto, Toronto, Ont., Canada, in 1975, 1977, and 1982, respectively.

In 1982 he was with INAOE, Mexico, as a Visiting Researcher in CAD. He then taught at the University of Toronto until 1992, when he moved to Carleton University, Ottawa, Ont., as a Professor and holder of the OCRI/NSERC Industrial Research Chair in High Speed Integrated Circuits. He spent sabbatical leaves in 1989 and 1990 as a Resident Visitor at AT&T Bell Laboratories in Reading, PA, working in CMOS analog design, and took research leaves in 1991 and 1992 to work on a VLSI circuits text, from which he taught at the University of Oulu, Finland. His work focuses on architectures and circuits for high-performance integrated circuits for signal processing applications. This includes RF signal conditioning, high-speed data conversion, real-time DSP, and CAD for signal processing.

Dr. Snelgrove was the winner of the 1986 Circuits and Systems Society Guillemin-Cauer Award for a 1986 paper coauthored with A. Sedra. He serves as an Associate Editor for the TRANSACTIONS ON CIRCUITS AND SYSTEMS II: ANALOG AND DIGITAL SIGNAL PROCESSING.